Peen forming and stress peen forming of 2024–T3 aluminum sheets. Part 2: eigenstrain analysis

Hong Yan Miao, Martin Levesque, Frédérick P. Gosselin

Laboratory for multiscale mechanics (LM2), Département de Génie Mécanique, Polytechnique Montréal, Montréal, QC, Canada

Abstract

In this study we use the theory of eigenstrains to investigate how different sources of anisotropy affected the results of shot peen forming experiments reported in Part 1. The specimens consisted of 4.9 mm thick 2024–T3 aluminum sheets uniformly shot peened on one face that were either free to deform or held onto a prestressing jig during peening. Potential sources of anisotropy included the plastic anisotropy of rolled aluminum, anisotropic initial stresses that redistribute when their equilibrium is disturbed by peenning, the geometry of the specimens, and externally applied prestress. For the alloy and peening conditions considered, plastic anisotropy had no discernable influence on the resulting shape of the peen formed specimens. Initial residual stresses, on the other hand, caused slightly larger bending loads in the rolling direction of the alloy. Although the magnitude of these loads was approximately 30 times smaller than peening-induced loads, it was sufficient to overcome the geometric preference for rectangular sheets to bend along their long side and cause all unconstrained specimens to bend along the rolling direction instead. Once the sheets started to deform, larger plastic strains developed in the bending direction. We show that this effect is equivalent to that used in the variant of the process called stress peen forming where parts are elastically prestressed during peening to obtain larger plastic strains in directions in which the material is stretched.

---

*Corresponding author

  Email address: `frederick.gosselin@polymtl.ca` (Frédérick P. Gosselin)
  URL: `http://www.polymtl.ca/lm2` (Frédérick P. Gosselin)

1. Introduction

Lower wing skins of most commercial aircraft are shaped using shot peen forming. The process consists in bombarding thin metal parts with hard shot, usually steel spheres less than one millimeter in diameter, propelled at velocities ranging from 20 to $100\,\mathrm{m\,s^{-1}}$ to plastically deform the material over a few tenths of a millimeter. In the plastically deformed layer, the material is compressed in the direction normal to the surface and stretched in the direction parallel to the surface, which causes the part to bend and elongate, as shown schematically in Figure 1a–b.

Although peen forming has been used since the 1950s, the literature review conducted in Part 1 Faucheux et al. (2021) found very few experimental studies of the process. It also highlighted two major limitations of these studies. First, the vast majority of publicly available data were acquired on 76×19 mm strips for peening conditions such that the deflection of the strips remained small when compared to their thickness. Consequently, these experiments did not capture nonlinear geometric effects that become significant when forming large panels (see Part 1 Faucheux et al. (2021)). Secondly, residual stresses were seldom measured in more than one direction even though several phenomena could induce anisotropic residual stresses. These include plastic anisotropy of the target material and prestress, a term used to designate external loads deliberately applied to a part being peened to increase plastic flow in directions in which the material is in tension. The manufacturing process of heat treatable aluminum plates in which most peen formed parts are machined is also known to induce anisotropic initial stresses that could affect the deformed shape of the parts and should, therefore, be characterized.

In Part 1 Faucheux et al. (2021), we reported the results of a peen forming experimental campaign designed to address these issues. The specimens consisted in 508 and 1016 mm long rectangular 2024–T3 aluminum sheets of different aspect ratios, sourced from the same lot, and peened with the same treatment. Some sheets were free to deform during peening while others were prestressed in a four-point bending jig. A noteworthy result was that

2
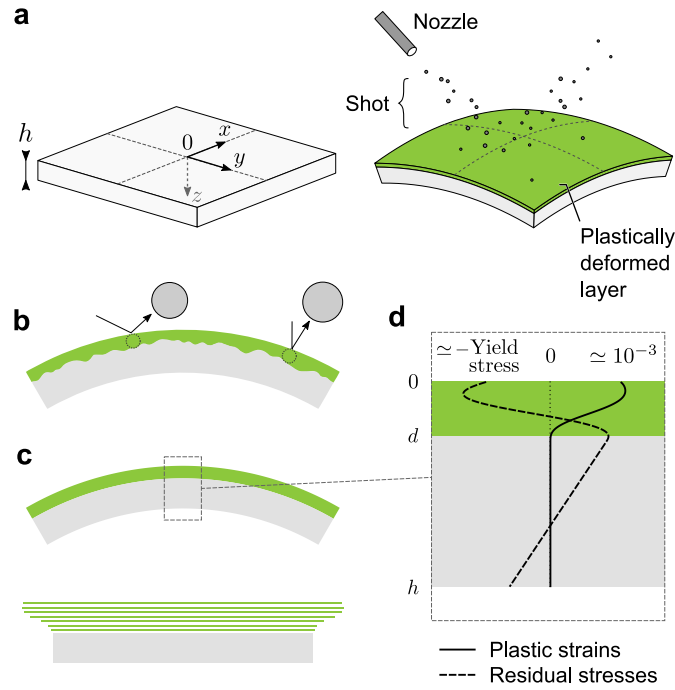
Figure 1. Peen forming of a metal plate. (a) Small and hard shot propelled at a metal surface at high velocity plastically deform a thin layer of material. As the material plastically flows in the direction parallel to the surface, it stretches the part and induces distortions. If controlled, this effect can be used to shape thin components. (b) At the scale of a shot, the distribution of plastic strains is highly irregular due to the stochastic nature of the process. (c) To visualize how plastic strains cause residual stresses and distortions, it is convenient to imagine cutting the plate into infinitesimally thin layers. In this (virtual) configuration, each layer is homogeneous, unconstrained, and therefore stress-free. Gluing the layers back together requires stretching some layers and compressing others, which induces internal stresses and distortions. (d) Typical in-plane plastic strain profiles after averaging in the plane of the plate. The profiles have a maximum at or near the surface and smoothly decrease to zero. Also shown is a typical in-plane residual stress profile.

all sheets that were free to deform bent in the rolling direction of the alloy, irrespective of their aspect ratio or of the peening trajectory. A similar phenomenon was reported in Kulkarni et al. (1981) for 2024 and 7075 aluminum although, in this case, 2024 aluminum specimens bent in the transverse direction of the alloy.

In a study about thin bilayers, Alben et al. (2011) showed that rectangular plates of uniform thickness made of an isotropically expanding active layer on top of a passive layer spontaneously bend along their long direction. This effect is purely geometrical and comes from regions of double curvatures that develop near the free edges, thus reducing the elastic energy of the system and making long side bending energetically favorable. That all our specimens bent along the rolling direction instead of the long direction therefore suggests that, for the alloy and peening conditions considered, material anisotropy was sufficiently strong to overcome this effect. In this article, we aim to clarify the contribution of each source of anisotropy to explain why all plates in Part 1 Faucheux et al. (2021) bent along the rolling direction.

The paper is structured as follows. After a brief summary of the experiments conducted in Part 1 Faucheux et al. (2021), Section 2 introduces the concept of eigenstrains on which the rest of the analysis is based. Section 3 presents equations needed to relate eigenstrains to residual stresses and strains in uniformly shot peened plates. Section 4 presents the procedures used to characterize eigenstrains present in our specimens as well as numerical models used to interpret the result. We then successively investigate the influence of prestress, plastic anisotropy, initial eigenstrains, and geometric effects on the deformed shape of the specimens in Sections 5 and 6.

2. Background

2.1. Summary of peen forming experiments conducted in Part 1 Faucheux et al. (2021)

All peen forming experiments reported in Part 1 Faucheux et al. (2021) were conducted on rectangular specimens cut from 4.9 mm thick 2024–T3 aluminum sheets from the same lot. Uniaxial tensile tests at 0, 45, and 90° from the rolling direction revealed isotropic elastic properties but a mild plastic anisotropy: the elastic modulus was 71 500 MPa and the yield stress at 0.2 % was 381 MPa along the rolling (L) direction, 349 MPa at 45° of the

4
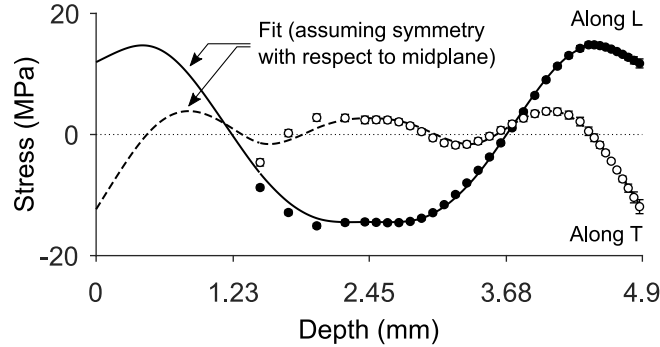
Figure 2. Residual stresses measured with the slitting method in 51×51 mm coupons removed from an as-rolled sheet.

rolling direction, and 339 MPa along the transverse (T) direction. Residual stresses in as-received sheets were measured with the slitting method. These initial stresses were anisotropic with a magnitude of less than 20 MPa both in tension and in compression, as shown in Figure 2.

Both conventional and stress peen forming experiments were conducted. For the former, specimens were free to deform during peening. For the latter, the specimens were elastically prestressed on the four-point bending jig shown in Figure 3a, shot peened, then released. Sheets of 1:4, 1:2, 1:1, 2:1, and 4:1 aspect ratio, here defined as the ratio of the dimension in the L direction to the dimension in the T direction, 1016 mm along their long side were used for conventional peen forming experiments. Smaller 508×127 mm strips were used for stress peen forming experiments. Prestress curvatures ranged from 0 (the strips were held flat) to 10.54×10^{-4} mm^{-1}, which corresponds to a radius of curvature of 949 mm.

All sheets were peened to full coverage in an automated compressed air peening cabinet with SCCW28 steel shot, 0.71 mm in diameter. The average velocity of shot exiting the nozzle was 41 m s^{-1}, which corresponds to an Almen intensity of 12.0 A(0.30 mmA). The treatment was applied progressively over the course of 12 peening cycles, each cycle delivering a small increment of coverage to the whole surface. For each geometry, one specimen was peened with strokes parallel to the L direction and another identical specimen was peened with strokes parallel to the T direction.

Figure 4 shows the final deformed shape of some of the sheets used for conventional peen forming experiments. All sheets, including those not shown,

5
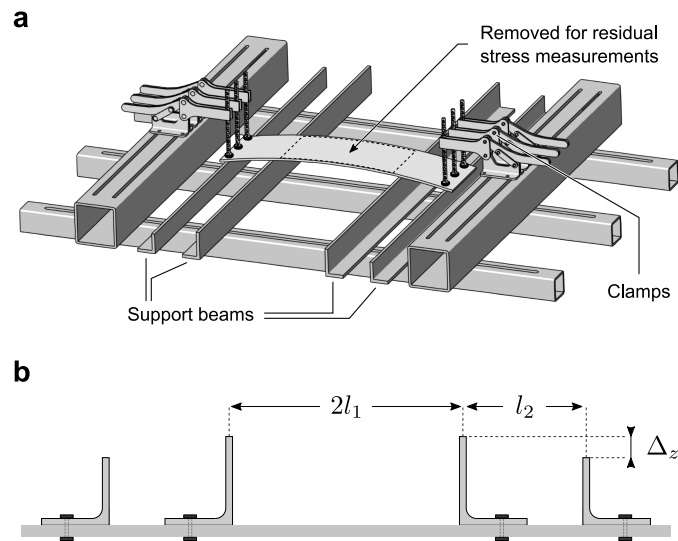
Figure 3. (a) Four-point bending jig used to hold 508×127 mm strips in a bent shape during stress peen forming experiments. The height and the spacing of the support beams could be varied to obtain different prestress curvatures. After peening, the strips were unclamped, their curvatures were measured, and a 254×127 mm coupon was removed from the central region for residual stress measurements. (b) Cross-sectional view of the jig. See supplementary material of Part 1 (Faucheux et al., 2021) for dimensions.
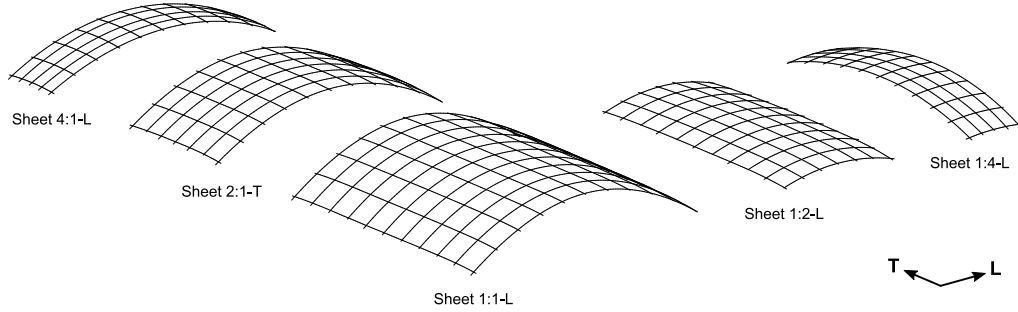
Figure 4. 3D scans of 4.9 mm thick and 1016 mm long 2024-T3 aluminum sheets of 4:1, 2:1, 1:1, 1:2, and 1:4 aspect ratio shot peened to full coverage with SCCW28 shot at an Almen intensity of $12.0\,\mathrm{A}(0.30\,\mathrm{mmA})$. The specimens were free to deform during peening. Deflection magnified by a factor of 4.

had their largest curvature along the L direction, irrespective of their aspect ratio or of the peening trajectory. While sheets of 1:1 and 2:1 aspect ratios deformed into cylindrical shapes with almost zero curvature in the T direction, other sheets assumed a compound curvature.

Because of size constraints, residual stresses could not be measured directly in as-peened specimens. Instead, smaller coupons were removed from the center of the specimens listed in Table 1 with a jigsaw and residual stresses were measured at the center of these coupons with the hole drilling method. Residual stresses were recorded at 51 µm intervals down to a depth of 1 mm and the data were fit with a sixth order polynomial to obtain continuous residual stress profiles.

The coupons, the dimensions of which were chosen as large as possible to minimize the effect of cutting induced plastic deformations and heating on measurement spots, were 254×254 mm for free-to-deform sheets and 254×127 mm for prestressed strips. Upon removal, stress rebalancing caused the coupons to deform. For example, sheet 1:1–L assumed a cylindrical shape with $3.46 \times 10^{-4}\,\mathrm{mm}^{-1}$ curvature in the L direction and almost zero curvature in the T direction while the coupon removed from it assumed an almost spherical shape with $2.93 \times 10^{-4}\,\mathrm{mm}^{-1}$ curvature in the L direction and $1.81 \times 10^{-4}\,\mathrm{mm}^{-1}$ curvature in the T direction. As a result, residual stresses measured in the coupons differed from those that would have been measured in as-peened specimens. Their analysis constitutes the bulk of the following sections.

Table 1

List of specimens peen formed in Part 1 (Faucheux et al., 2021) for which residual stress measurements are available.

Specimen ID	Dimensions		Prestress curvature ($\times 10^{-4}$ mm)
	Along L (mm)	Along T (mm)	
Sheet 4:1–L	1016	254	
Sheet 2:1–T	1016	508	Free to deform
Sheet 1:1–L	1016	1016	
Sheet 1:2–L	508	1016	
Sheet 1:4–L	254	1016	
Strip K0–L–A	508	127	0
Strip K1–L–A	508	127	2.82
Strip K2–L–A	508	127	5.11
Strip K3–L–A	508	127	8.28
Strip K4–L–A	508	127	10.54

2.2. Eigenstrains

Recall that our aim is to clarify the contribution of different sources of anisotropy on the final deformed shape of the aluminum sheets peen formed in Part 1 (Faucheux et al., 2021). This analysis must be carried out from the only experimental data available, namely residual stresses and curvatures measured on coupons removed from the specimens. Because of stress rebalancing, these stresses and curvatures differ from those in the original specimens. On the other hand, if the coupon were carefully removed, and provided that no reverse yielding occurred during springback, then plastic strains were not affected by this removal. Consequently, characterizing plastic strains in the coupons provides a direct means to study the effect of the peening treatment on the original specimens.

At the scale of a shot, the distribution of plastic strains induced by shot peening treatments is highly irregular as it depends on the precise sequence of impacts and on the distribution of impact velocities. On average, however, symmetry and translational invariance require that the plastic strain field ε^{pl} only depends on the coordinate normal to the surface and that shear components be zero. In the rectangular coordinate system of Figure 1a, this

implies that

$$\boldsymbol{\varepsilon}^{pl}(z) = \begin{pmatrix} \varepsilon_{xx}^{pl}(z) & 0 & 0 \\ 0 & \varepsilon_{yy}^{pl}(z) & 0 \\ 0 & 0 & \varepsilon_{zz}^{pl}(z) \end{pmatrix}. \tag{1}$$

Furthermore, the fact that plastic deformations take place at constant volume requires that $\varepsilon_{zz}^{pl} = -(\varepsilon_{xx}^{pl} + \varepsilon_{yy}^{pl})$. Since peening stretches the material in the direction parallel to the surface and compresses it in the direction normal to the surface, ε_{xx} and ε_{yy} are positive while ε_{zz} is negative.

To visualize what residual stresses and distortions a peening treatment does induce, it is convenient to imagine cutting a shot peened part into infinitesimally thin layers parallel to its surface and letting the system relax, as shown schematically in Figure 1c. In this virtual configuration, the layers are not constrained by surrounding material; the strains they undergo are equal to the plastic strains and residual stresses are zero everywhere. Since the strains from one layer to the next are incompatible, reassembling the structure requires stretching some layers and compressing others, which induces residual stresses and distortions. Figure 1d shows typical plastic strain and residual stress profiles in uniformly shot peened plates. Plastic strains are the largest at, or near, the peened surface then gradually decrease to zero. Residual stresses vary linearly in the bulk owing to the bending and stretching of the plate. They reach a maximum near the transition with the peening-affected layer, located at $z = d$, then decrease until they become compressive near the surface.

There exist a general framework to study the relationship between incompatible strains, residual stresses, and distortions called the theory of eigenstrains (Korsunsky, 2017). The term eigenstrains refers to all permanent nonelastic strains present in a structure. Thus, for small strains

$$\boldsymbol{\varepsilon} = \boldsymbol{\varepsilon}^{el} + \boldsymbol{\varepsilon}^*, \tag{2}$$

where $\boldsymbol{\varepsilon}$ are the total strains, $\boldsymbol{\varepsilon}^{el}$ are the elastic strains, and $\boldsymbol{\varepsilon}^*$ are the eigenstrains. Similarly, the eigenstrains can themselves be additively decomposed into thermal strains, plastic strains, and any other source of nonelastic strains. Many analytical solutions have been reported that relate specific distributions of eigenstrains to the residual stresses and distortions they induce, some of which are reviewed in Mura (1987). Conversely, several authors addressed the inverse problem of identifying eigenstrains present in a structure

9

from limited experimental measurements; see for example in Jun and Korsunsky (2010). Since plastic deformation is the only source of eigenstrains in shot peened parts, these inverse identification procedures can be used without modifications to compute peening-induced plastic strains. Therefore, here we consider $\boldsymbol{\varepsilon}^* = \boldsymbol{\varepsilon}^{pl}$.

In general, identifying eigenstrains is an iterative process that involves finite element simulations and optimization algorithms. For simple geometries, however, closed-form solutions that relate eigenstrains to residual stresses and total strains are available.

3. A model to relate eigenstrains, stresses, and strains in uniformly shot peened plates

Consider a plate of uniform thickness h, made of an isotropic material with elastic modulus E and Poisson ratio ν, and subjected to a distribution of eigenstrains of the form of Equation (1). Using the coordinate system of Figure 1a, let

$$\alpha_i = \int_0^h \varepsilon_{ii}^*(z)\mathrm{d}z \quad \text{and} \quad \beta_i = \int_0^h \varepsilon_{ii}^*(z)\, z\mathrm{d}z, \quad i = \{x, y\} \tag{3}$$

be the resulting eigenstrains and the first eigenstrains moment with respect to the peened surface. Within the hypotheses of the theory of linear elasticity, (residual) stresses $\boldsymbol{\sigma}$ are related to the strains through

$$\varepsilon_{xx} = a_x z + b_x, \qquad\qquad\qquad \varepsilon_{yy} = a_y z + b_y, \tag{4}$$

$$\varepsilon_{xx}^{el} = \varepsilon_{xx} - \varepsilon_{xx}^*, \qquad\qquad\qquad \varepsilon_{yy}^{el} = \varepsilon_{yy} - \varepsilon_{yy}^*, \tag{5}$$

$$\sigma_{xx} = \frac{E}{1-\nu^2}\left[\varepsilon_{xx}^{el} + \nu\varepsilon_{yy}^{el}\right], \qquad \sigma_{yy} = \frac{E}{1-\nu^2}\left[\varepsilon_{yy}^{el} + \nu\varepsilon_{xx}^{el}\right], \tag{6}$$

where

$$a_i = \left(12\beta_i - 6\alpha_i h\right)/h^3, \qquad b_i = \left(4\alpha_i h - 6\beta_i\right)/h^2. \tag{7}$$

This solution can be derived by adopting the kinematic assumption of Equation (4) – material lines perpendicular to the undeformed midsurface remain straight during deformation – and by using the stress-strain relation of Equation (6) to enforce that resulting axial loads and bending moments acting on any cut through the plate must be zero, as was done in Korsunsky (2005)

10

for equibiaxial eigenstrains. Another derivation without a priori kinematic assumptions is presented in the supplementary material.

In this simple case, the above equations can be inverted to yield the eigenstrains in terms of residual stresses and total strains. Solving Equation (6) for the strains yields

$$\varepsilon_{xx}^{el} = (\sigma_{xx} - \nu\sigma_{yy})/E, \qquad \varepsilon_{yy}^{el} = (\sigma_{yy} - \nu\sigma_{xx})/E. \tag{8}$$

Finally, combining Equations (4), (5), and (8), and noticing that

$$a_i = -\kappa_i, \tag{9}$$

where κ_i is the curvature of the plate in the i direction, yields

$$
\begin{aligned}
\varepsilon_{xx}^* &= \left(\varepsilon_{xx}\big|_{z=0} - \kappa_x z \right) - (\sigma_{xx} - \nu\sigma_{yy})/E, \\
\varepsilon_{yy}^* &= \left(\varepsilon_{yy}\big|_{z=0} - \kappa_y z \right) - (\sigma_{yy} - \nu\sigma_{xx})/E,
\end{aligned}
\tag{10}
$$

where $\boldsymbol{\varepsilon}\big|_{z=0}$ are total strains measured on the upper face of the plate.

4. Methods

4.1. Near-surface eigenstrains

The near-surface eigenstrains present in our specimens were computed from residual stress and curvature measurements using Equation (10). Here and in what follows, we used $E = 71500$ MPa and $\nu = 0.33$. Because the in-plane stretch of the coupons by the peening treatment has not been characterized, the constant terms $\varepsilon_{ii}\big|_{z=0}$ in Equation (10) could not be determined directly. To enable comparing eigenstrain profiles, the missing constant was set such that the eigenstrains were equal to zero at the end of the peening-affected layer, that is, $\varepsilon_{ii}^*(d) = 0$, as shown in Figure 5a. Since residual stress measurements showed that d varied little across specimens, we used $d = 0.5$ mm in all cases. (Recall from Section 2.2 that the depth of the peening-affected layer can be estimated from the location of the tensile residual stress peak; also see Korsunsky (2005).) Although it is sensitive to experimental errors and oscillations in the profiles, this approach is sufficient for the purpose of this analysis.
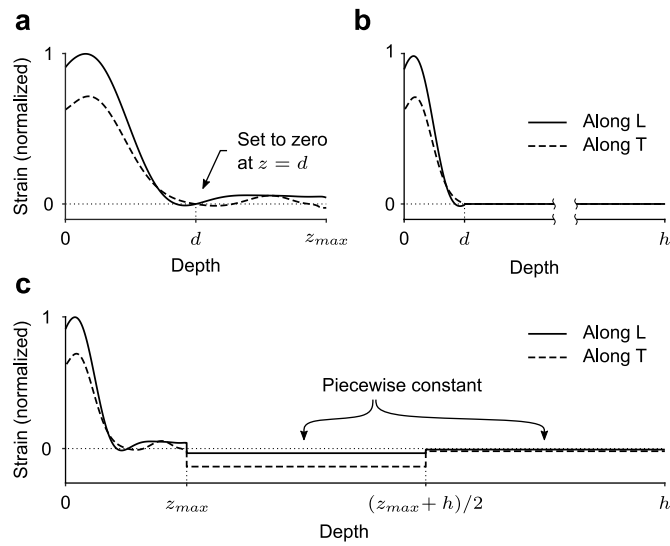
Figure 5. Typical eigenstrain profiles. (a) Near-surface eigenstrains computed from curvature and residual stress measurements using Equation (10). (b) Peening-induced eigenstrains obtained by truncating the profiles in (a) at the end of the peening affected layer. (c) Through-thickness profiles obtained by extending the profiles in (a) with piecewise constant functions. The magnitude of the piecewise constant parts is chosen such that if these profiles were input in a model of a small coupon, they would induce the same axial stretch and the same curvatures as those that would be measured.

4.2. Accounting for initial eigenstrains

Equation (10) only returns eigenstrain profiles up to the depth at which residual stresses have been measured—in this case $z_{max} = 1$ mm. However, the shape of residual stress profiles measured in as-rolled sheets (Figure 2) indicates that anisotropic incompatible eigenstrains are initially present through the entire thickness of the specimens.

To estimate how eigenstrains deeper than z_{max} affected the final deformed shape of free-to-deform specimens, we first input the previously identified peening-induced eigenstrains, i.e., only the $z < d$ part or the profiles, into a finite element model of the specimens and solved for equilibrium. Figure 5b shows a typical profile used for these simulations. This provided an estimate of the shape that the specimens would have assumed if no initial eigenstrains were present. These results were then compared to a second set of simulations that included the contribution of initial eigenstrains.

A simple way to perform these simulations consists in constructing idealized eigenstrain profiles $\hat{\varepsilon}_{ii}^*(z)$ that, when input into a model of the coupons, induce the same in-plane stretch and the same curvatures as those that were experimentally measured, then to input these profiles into a model of the sheets. This process may be interpreted as reassembling a sheet by joining together several coupons, as illustrated in Figure 6; it is the opposite of coupons removal.

Since all quantities are explicitly integrated over the thickness in conventional thin plate theories, any eigenstrain profiles having the same resulting values and first moments will yield the same deformed shape. Therefore, the only conditions that idealized profiles must satisfy to induce the desired axial stretch and curvatures is

$$\int_0^h \hat{\varepsilon}_{ii}^*(z)\mathrm{d}z = \alpha_i, \qquad \int_0^h \hat{\varepsilon}_{ii}^*(z)\,z\mathrm{d}z = \beta_i, \qquad i = \{x, y\}. \qquad (11)$$

In what follows, we use

$$\hat{\varepsilon}_{ii}^*(z) = \begin{cases} \breve{\varepsilon}_{ii}^*(z) & \text{if } z \leq z_{max}, \\ \theta_i^{top} & \text{if } z_{max} < z \leq (z_{max} + h)/2, \\ \theta_i^{btm} & \text{if } (z_{max} + h)/2 < z \leq h, \end{cases} \qquad (12)$$

where $\breve{\varepsilon}_{ii}^*$ are the eigenstrains identified in Section 4.1 and θ_i^{top} and θ_i^{btm} are

13

constants evaluated to satisfy Equation (11). Figure 5c shows a typical profile obtained in this way. The reason for choosing such profiles instead of simpler ones is that, by construction, they not only induce the correct deformations but also the correct residual stresses in the $z \leq z_{max}$ region. Consequently, they enable estimation residual stresses present in the $z \leq z_{max}$ region of the original sheets before the coupons were removed—in other words, to correct for the stress relaxation that occured during removal. An explicit expression for the constants can be obtained by substituting Equation (12) into (11), integrating, and solving for the constants. This yields

$$
\begin{aligned}
\theta_i^{\text{top}} &= \quad [(\alpha_i - \check{\alpha}_i)(3h + z_{max}) - 4(\beta_i - \check{\beta}_i)]/(h - z_{max})^2, \\
\theta_i^{\text{btm}} &= -[(\alpha_i - \check{\alpha}_i)(3z_{max} + h) - 4(\beta_i - \check{\beta}_i)]/(h - z_{max})^2,
\end{aligned}
\tag{13}
$$

where

$$
\check{\alpha}_i = \int_0^{z_{max}} \check{\varepsilon}_{ii}^*(z)\mathrm{d}z \qquad \text{and} \qquad \check{\beta}_i = \int_0^{z_{max}} \check{\varepsilon}_{ii}^*(z)\, z\mathrm{d}z.
\tag{14}
$$

Finally, using the inverse of Equation (7),

$$
\alpha_i = (a_i h^2 + 2b_i h)/2, \qquad \beta_i = (2a_i h^3 + 3b_i h^2)/6,
\tag{15}
$$

and recalling that $a_i = -\tilde{\kappa}_i$ and $b_i = \tilde{\varepsilon}_{ii}|_{z=0}$, where a 'tilde' is used to indicate that a quantity is measured on a coupon, the constants can be expressed in terms of quantities that can be determined experimentally.

Again, because the in-plane stretch of the coupons had not been characterized, the value of $\tilde{\varepsilon}_{ii}|_{z=0}$ was unknown. However, for moderately curved *uniformly* shot peened plates, this term has very little influence on computed curvatures and residual stresses. Indeed, it has the same effect as an homogenous in-plane expansion which, by analogy with homogenous thermal expansion, only causes the structure to expand without inducing stresses. In fact, curvatures are independent of $b_i \, (= \tilde{\varepsilon}_{ii}|_{z=0})$ in the linear domain, that is, for very small curvatures, as shown by Equation (9). In what follows, we arbitrarily used $\tilde{\varepsilon}_{ii}|_{z=0} = \kappa_i h/2$, which corresponds to a scenario where the midplane of the plates does not stretch. Running the simulations for any $\tilde{\varepsilon}_{ii}|_{z=0}$ in the $\pm\, 5 \times 10^{-3}\, \text{mm mm}^{-1}$ range, where $5 \times 10^{-3}\, \text{mm mm}^{-1}$ is the typical magnitude of peening induced eigenstrains (see later sections), yielded virtually identical results.

14
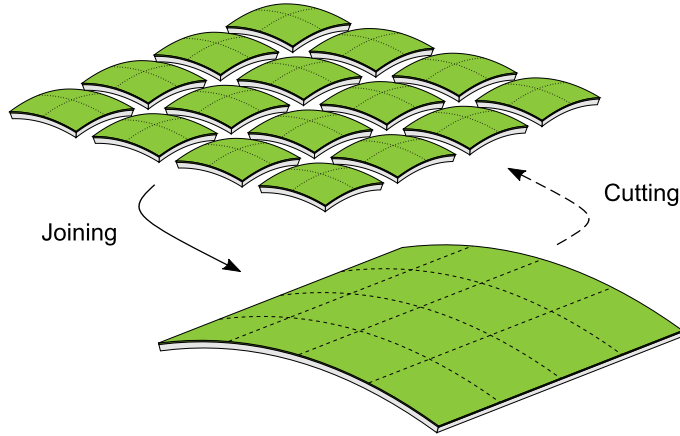
Figure 6. Thought experiment where a large peen formed plate is cut into many small coupons and the coupons are then joined back together. If neither cutting nor springback induce plastic deformation, then the process is reversible.

4.3. Finite element simulations

All finite element simulations were done with Abaqus 6.14. Taking advantage of symmetries, only one quarter of the geometries were meshed, as shown in Figure 7a. Eigenstrain profiles were input as pseudo-thermal strains with the UEXPAN subroutine as described in Jun and Korsunsky (2010). The distribution of integration points through the thickness was as shown in Figure 7c, with 99 integration points over $0 \leq z \leq z_{max}$, 3 integration points over $z_{max} \leq z \leq (z_{max} + h)/2$, and 3 integration points over $(z_{max} + h)/2 \leq z \leq h$. Geometric nonlinearities were included in all analyses. Gravity was neglected as additional simulations showed that it caused variations in curvatures of less than $5\,\%$.

Similar simulations were used to compute residual stresses in prestressed strips while the strips were still held onto the prestressing jig. Figure 7b shows the 1/4th symmetry model used for these simulations. The contact between the strips, clamps, and support beams was modeled by prescribing z-displacements along the lines where the strips touched support beams.

4.4. Definitions

To facilitate the discussion, we first introduce relevant dimensionless parameters. As discussed in Audoly and Pomeau (2010), it is usually possible
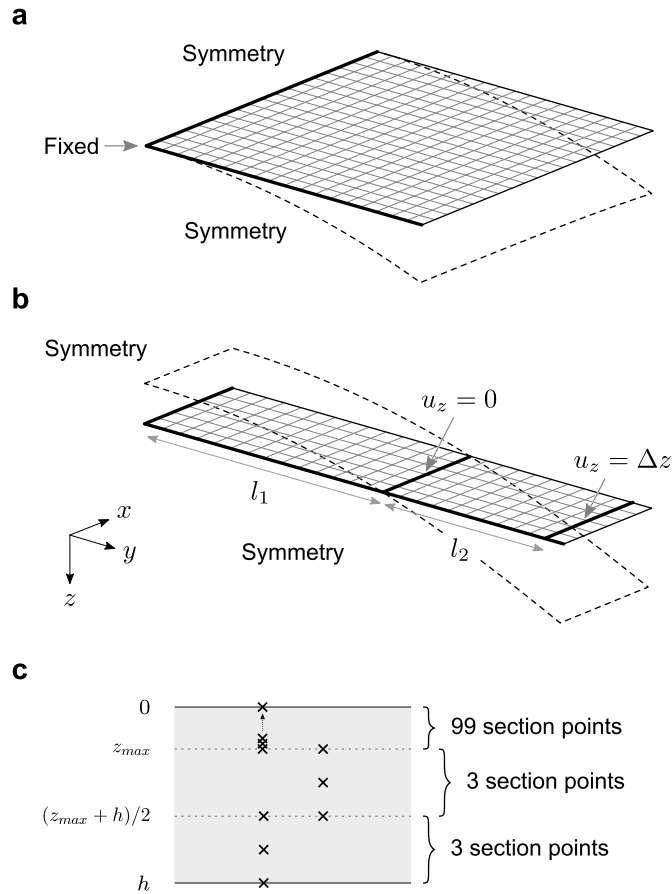
Figure 7. Finite element models used to simulate (a) conventional peen forming and (b) stress peen forming experiments. For the latter model, contact between prestressed strips, clamps, and support beams was modeled by prescribing z-displacements along the lines where the strips touched support beams (see Figure 3). The mesh used for simulations was three times finer than that shown, i. e., had 9 times more elements. (c) Distribution of integration points through the thickness of the shell elements.

16

to characterize the response of thin structures with very few dimensionless parameters with the same parameters being valid for both small and large deformations. Here, we propose to use

$$\bar{B} = 12(1+\nu)B_{avg}L^2/h^4, \quad \chi = (B_{long} - B_{avg})/B_{avg}, \quad \bar{\kappa} = \kappa L^2/h, \quad \nu, \quad (16)$$

where L is a characteristic length (here taken as the dimension along the longest side), h is the thickness, κ is any curvature measured on the plate,

$$B_{avg} = (B_{long} + B_{short})/2, \tag{17}$$

and B_{long} and B_{short} are the first eigenstrain moments with respect to the midplane of the plate in the long and short directions. Using the axis convention of Figure 1a, the first eigenstrain moment with respect to the midplane of the plate along the i direction is given by

$$B_i = \int_0^h \varepsilon_{ii}^*(z)(h/2 - z)\mathrm{d}z. \tag{18}$$

The parameter $\bar{B}$ corresponds to the ratio of bending loads over bending rigidity rescaled by $(L/h)^2$, χ characterizes the anisotropy of eigenstrains, and $\bar{\kappa}$ is a dimensionless curvature.

Simple idealized eigenstrain profiles of the form

$$\varepsilon_{ii}^*(z) = \begin{cases} \theta_i & \text{if } z \leq h/2, \\ -\theta_i & \text{if } z > h/2, \end{cases} \tag{19}$$

where

$$\theta_i = \frac{\bar{B}h^3}{3(1+\nu)L^2}(1+\chi) \tag{20}$$

in the long direction and

$$\theta_i = \frac{\bar{B}h^3}{3(1+\nu)L^2}(1-\chi) \tag{21}$$

in the short direction were used to obtain the desired dimensionless loads and χ.

17

5. Results

The left panels of Figures 8 and 9 show near-surface eigenstrains identified in the coupons removed from free-to-deform and prestressed strips, respectively. The shape of the profiles is typical of that induced by peening treatments: eigenstrains peak at or near the peened surface then decrease gradually until they reach a plateau, approximately 0.5 mm below the surface, which corresponds to the end of the peening-affected layer. In all cases, eigenstrains are larger in the directions in which the specimens bent the most, that is, along the L direction for free-to-deform sheets, and along the prestress direction for prestressed strips.

Inputting these eigenstrains (including the piecewise constant extension not shown in the figures) into a model of the coupons yields the residual stresses shown as solid lines in the middle panels. In all cases, computed stresses match experimental data, which confirms that eigenstrains present in the coupons were correctly identified.

Estimates of residual stresses in the original specimens, prior to coupons removal, are shown in the right panels. For free-to-deform specimens, the only apparent difference between these profiles and those in the coupons is that residual stresses in the L and T directions in sheets 1:1–L and 2:1–T become almost superimposed over the first 0.2 mm below the peened surface owing to the bending of the specimens. Similarly, residual stresses in the L and T direction of prestressed strips are closer to one another than residual stresses in the coupons and they exhibit almost the same minimum in both directions.

Finally, Table 2 lists experimentally measured and simulated curvatures for free-to-deform sheets. The relative error RE is defined as:

$$\text{RE} = \frac{\kappa_{i_{sim}} - \kappa_{i_{exp}}}{\frac{1}{2}(\kappa_{x_{exp}} + \kappa_{y_{exp}})} \times 100\%, \tag{22}$$

where $i = \{x, y\}$ and represents the L and T directions, $\kappa_{i_{sim}}$ and $\kappa_{i_{exp}}$ are simulated and experimental curvatures in L and T directions, respectively. These simulations qualitatively reproduce the response of the sheets. The relative error between measured and simulated curvatures ranges between -20 and 15% in the L direction and between -25 and 4% in the T direction. On the other hand, simulations that neglected the contribution of initial eigen-

18
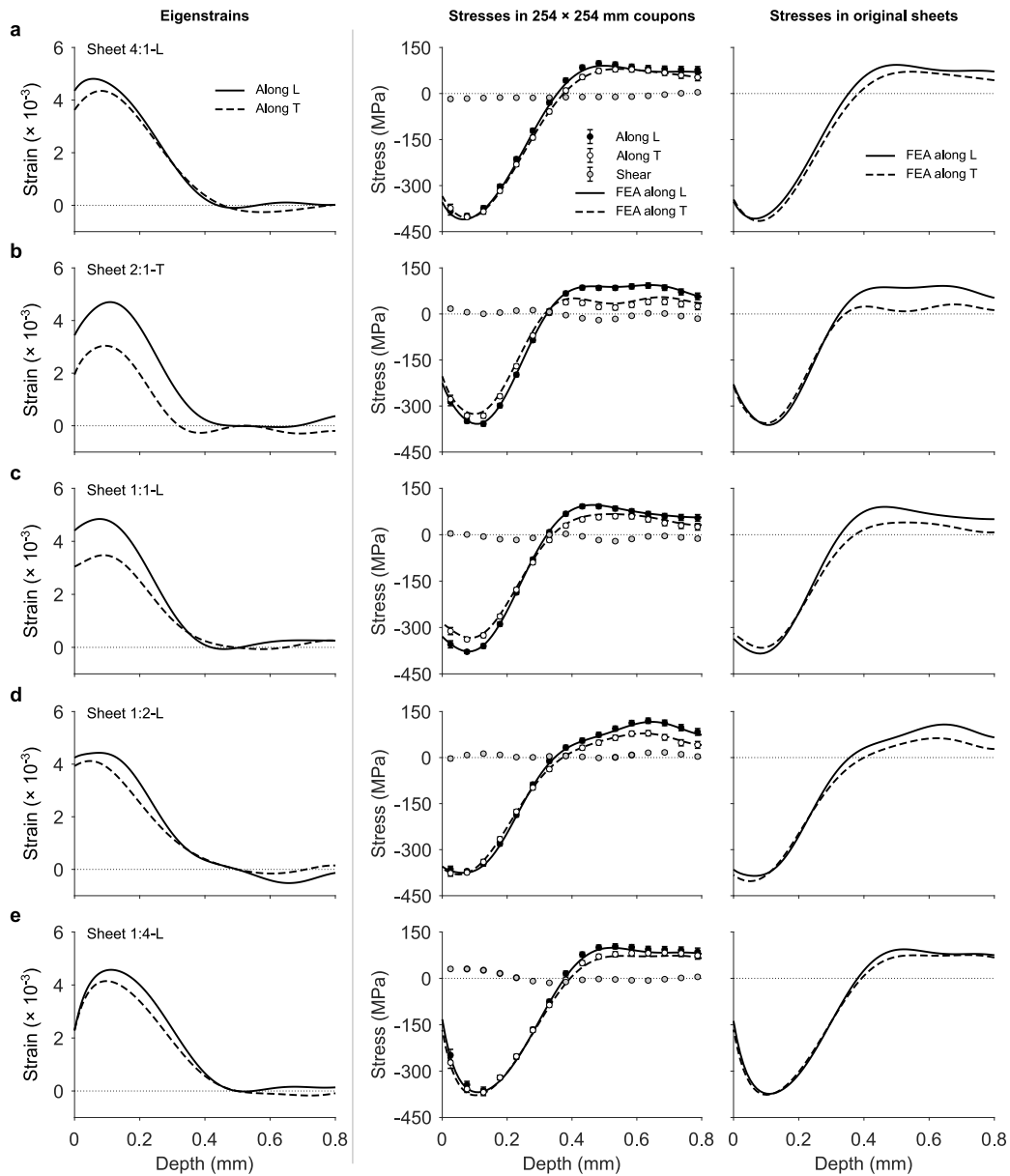
Figure 8. Eigenstrains and residual stresses in specimens used for conventional peen forming experiments. Left: Peening-induced eigenstrains. Middle: Residual stresses measured with the hole drilling method at the center of the coupons. Also shown are residual stresses obtained when the complete eigenstrain profiles (i.e., after they were extended to include the contribution of initial eigenstrains; see Section 2.2) are input into a finite element model of the coupons. Right: Residual stresses in the sheets prior to removal of the coupons—estimated by inputting the same eigenstrain profiles into finite element models of the sheets.

19
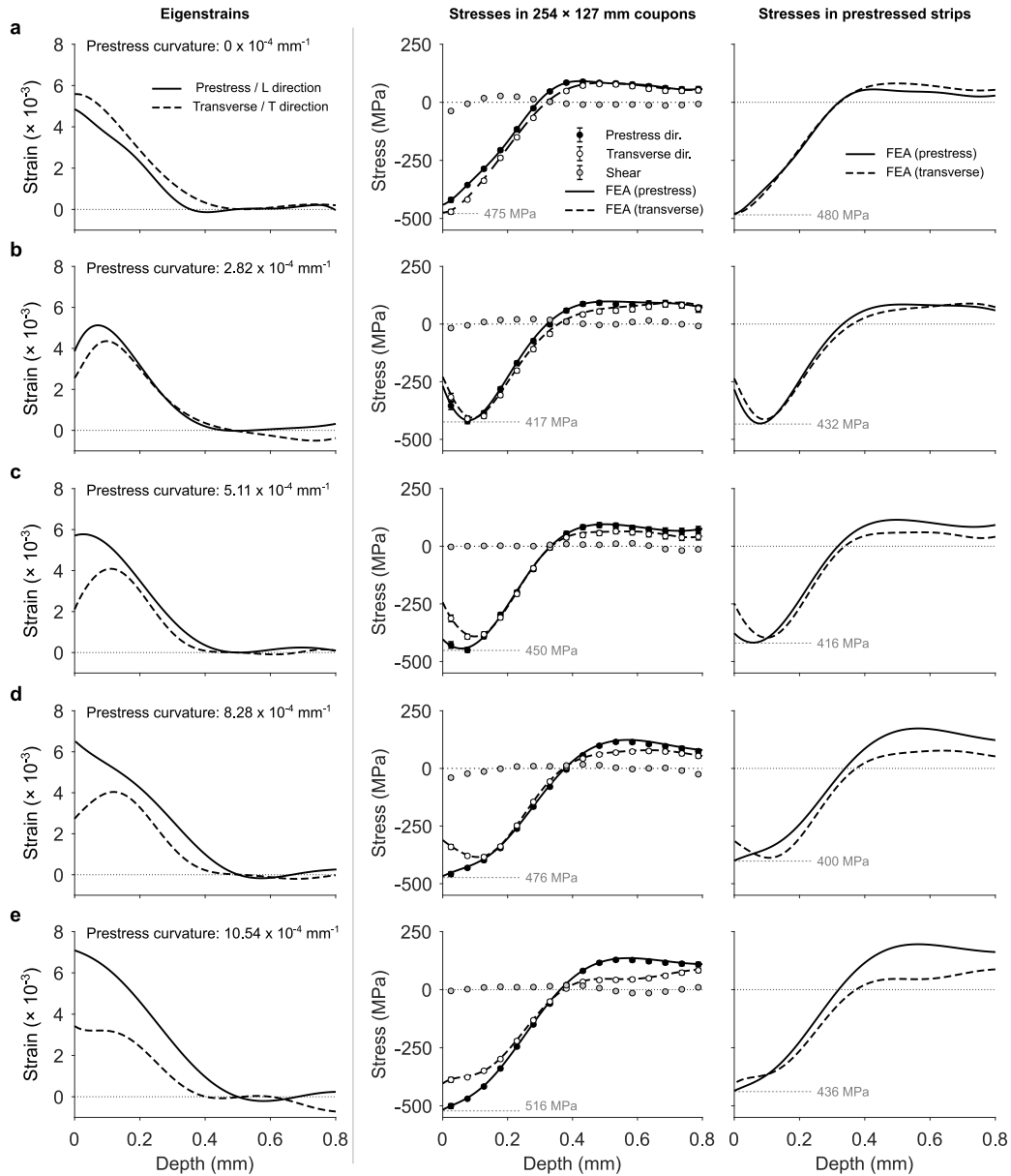
Figure 9. Eigenstrains and stresses in specimens used for stress peen forming experiments. Left: Peening-induced eigenstrains. Middle: Residual stresses measured with the hole drilling method at the center of the coupons and residual stresses obtained when the complete eigenstrain profiles are input into a finite element model of the coupons. Right: Stresses in the sheets prior to removal of the coupons while the sheets are still held on the prestressing jig—estimated by inputting the same eigenstrain profiles into finite element models of the strips.

20

Table 2

Experimental and simulated curvatures of sheets used for conventional peen forming experiments.

Specimen	Experimental curvatures $\kappa_{i_{exp}}$ ($\times 10^{-4}$ mm^{-1})		Simulated curvatures $\kappa_{i_{sim}}$ ($\times 10^{-4}$ mm^{-1})				Relative error RE (%)			
			Including initial eigenstrains		Neglecting initial eigenstrains		Including initial eigenstrains		Neglecting initial eigenstrains	
	Along L	Along T	Along L	Along T	Along L	Along T	Along L	Along T	Along L	Along T
Sheet 4:1–L	2.50	2.19	2.54	1.72	2.18	2.27	2	-20	-14	3
Sheet 2:1–T	3.06	0.11	3.30	0.03	2.30	0.28	15	-5	-48	11
Sheet 1:1–L	3.46	−0.01	3.25	−0.07	2.64	−0.08	-12	-3	-48	-4
Sheet 1:2–L	3.56	0.30	3.18	0.38	0.40	2.18	-20	4	-164	97
Sheet 1:4–L	3.00	1.81	3.07	1.24	2.26	2.65	3	-25	-31	33

strains display larger errors in most of the cases. Errors range from -164 to -14% in the L direction and from -4 to 97% in the T direction. The curvatures of prestressed strips (not shown) were identical to prestress curvatures as jig constraints prevented the strips to deform. The fact that simulations that included the contribution of initial eigenstrains do not perfectly match experiments suggests that some plastic yielding occurred during coupons removal. Indeed, experimental and simulated deformed shapes should be identical if eigenstrains in the coupons and in the sheets were the same.

6. Discussion

6.1. Influence of prestress

That larger eigenstrains developed in the direction in which specimens bent the most confirms that prestress, whether it results from externally applied loads or from the progressive deformation of an unconstrained specimen, does affect the distribution of peening-induced plastic strains. This is further evidenced by Figure 10 which shows the same eigenstrain profiles as in Figure 9 but superimposed. Whereas eigenstrains along the transverse direction are almost superimposed, the magnitude of eigenstrains along the prestress direction increases with prestress curvature. Similar results were reported by Hu et al. (2015) for laser peening simulation of 2024–T3 aluminum sheets. Similarly, sheets 2:1–T and 1:1–L, which deformed into cylindrical shapes, display larger eigenstrains along the bending (L) direction whereas other unconstrained sheets, which deformed into elliptical or nearly spherical shapes, display similar eigenstrains in both directions (see Figure 8).

a Along prestress direction

Strain ($\times 10^{-3}$)

Prestress curvature
($\times 10^{-4}$ mm^{-1})

10.5	
8.3	
5.1	
2.7	
0	

b Along transverse direction

Strain ($\times 10^{-3}$)

Depth (mm)
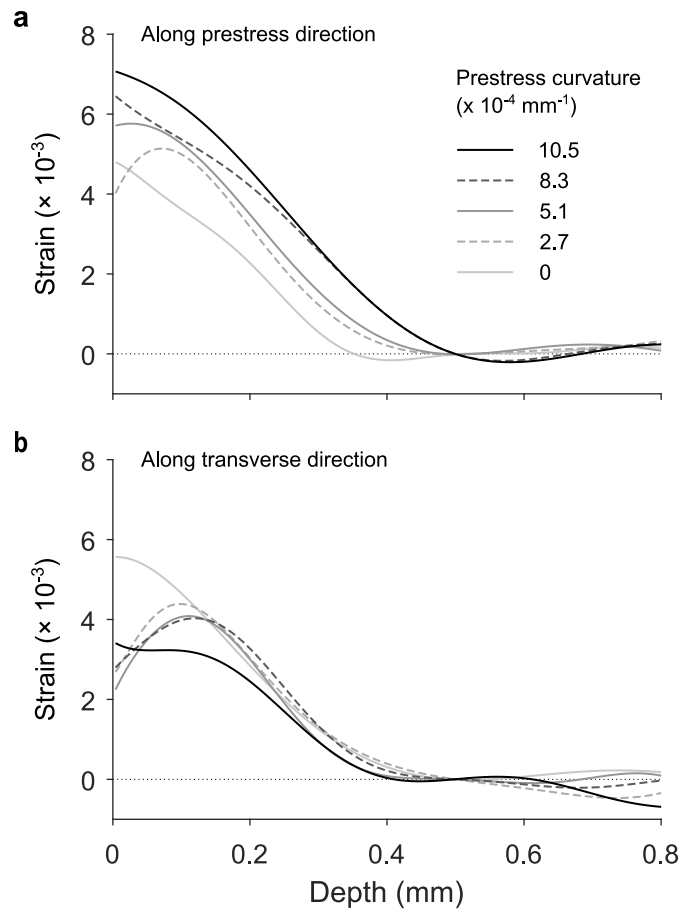
Figure 10. Peening-induced eigenstrains in stress peen formed strips.

Although it can induce anisotropic eigenstrains, prestress alone, however, does not explain why all unconstrained specimens bent in the same direction. Consider for example the 1:1 aspect ratio sheet shown in Figure 4. This sheet was peened with strokes parallel to the L direction and bent in L direction. If prestress alone did determine the bending direction, we would expect an identical sheet peened in the same conditions with strokes parallel to the T direction to bend along T. Experiments conducted in Part 1 (Faucheux et al., 2021) showed that this was not the case; all specimens bend along L, irrespective of the peening trajectory.

6.2. Influence of plastic anisotropy

One phenomenon that could explain why unconstrained specimens preferentially bent in the L direction is the known plastic anisotropy of the 2024–T3 aluminum alloy (Bron and Besson, 2004; Seidt and Gilat, 2013). Mild plastic anisotropy was observed during uniaxial tensile tests conducted in Part 1 Faucheux et al. (2021). Clear evidence of how indenting a mildly plastically anisotropic material can result in a highly anisotropic response was reported in Prime (2017) where the authors measured residual stresses 40 % larger in the T direction than in the L direction at the center of a 10 mm thick 2024–T3 aluminum disk after it had been indented with two opposing cylindrical punches. This result was attributed to preferential plastic flow along the T direction as compression tests showed that stress-strain curves in the T direction were about 40 MPa below the curves in the L direction. Uniaxial compression tests reported in Seidt and Gilat (2013) for plates of the same alloy and thickness also identified the T direction as the weaker one, as did the tensile tests of Part 1 Faucheux et al. (2021). These observations, however, should not be used be extrapolate the behavior of heavily shot peened specimens since laboratory tests do not capture the effect of the complex loading paths experienced by material points close to the peened surface.

Whether plastic flow occurred preferentially in the L or T direction can be assessed from eigenstrain profiles in the strip that was held flat during peening (Figure 9a). For this strip, curvatures, hence the effect of prestress, were the same in all directions. Consequently, any observed anisotropy in near-surface eigenstrains would result from plastic anisotropy. Similarly, markedly anisotropic eigenstrains in free-to-deform 1:4 and 4:1 aspect ratio specimens (Figure 8a, e) would betray plastic anisotropy since the geometry of these specimens constrains them to deform into quasi-spherical shape, thus induc-
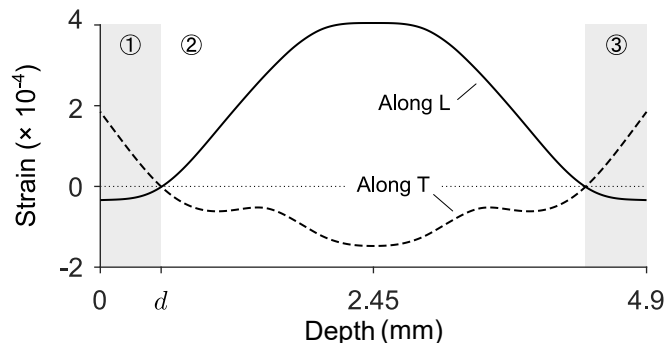
Figure 11. Eigenstrains in an as-received sheet computed from the residual stress profiles in Figure 2 using Equation 10. When a plate in which such eigenstrains are initially present is peened on the face located at $z = 0$, initial eigenstrains in the peening affected layer (region 1) are replaced by positive peening-induced eigenstrains about one order of magnitude larger than initial eigenstrains which causes the structure to bend. Eigenstrains present deeper into the material are left unaffected by the treatment.

ing approximately the same prestress in all directions. The profiles, however, show no clear sign of plastic anisotropy that would favor L side bending: eigenstrains are almost the same in both directions in free-to-deform specimens and they are slightly larger in the T direction for the specimen held flat during peening, which does favor T side bending.

6.3. Influence of initial eigenstrains

Another source of material anisotropy that could explain why free-to-deform specimens bent along the L direction is initial eigenstrains.

Figure 11 shows eigenstrains in an as-rolled sheet computed from the initial stress profiles in Figure 2 using Equation (10). If a specimen in which these eigenstrains are initially present is peened on the surface located at $z = 0$, large positive eigenstrains will develop in the peening affected layer and induce positive curvatures. Initial eigenstrains present deeper into the material, however, are left unaffected by the treatment. Let d be the depth the peening-affected layer. Because they are symmetric with respect to the midplane of the plate, initial eigenstrains in the $d \leq z \leq h - d$ region (region 2) induce no bending loads hence have no effect on curvatures. On the other hand, eigenstrains in the $z \geq h - d$ region (region 3) decrease curvatures if they are positive and increase curvatures if they are negative.

In this case, eigenstrains in region 3 are slightly larger in the T direction than

in the L direction, thus favoring L side bending. However, their magnitude, hence the bending moment they induce, is one to two order of magnitude smaller than peening-induced eigenstrains. Although this suggests that initial eigenstrains have very little influence on the final deformed shape of the specimens, finite element simulations summarized in Table 2 showed that this was not the case as neglecting initial eigenstrains caused simulated curvatures to vary by several tens of percent for all specimens and caused an inversion in the bending direction of the 1:2 aspect ratio sheet. Considering the low magnitude of initial eigenstrains, these results show that the response of uniformly shot peened plates, and in particular that of 1:2 aspect ratio plates, is highly sensitive to small variations in eigenstrains.

6.4. Competition between geometric effects and eigenstrains anisotropy

This sensitivity is surprising since, for specimens of aspect ratio smaller than one, L side bending can only occur if the eigenstrains are sufficiently anisotropic to compete against the geometric preference of rectangular sheets to bend along their long direction. This effect, which was described in Alben et al. (2011), comes from regions of double curvatures that develop near the free edges of plates loaded with biaxial eigenstrains and that lowers the elastic energy of the system, thereby making long side bending energetically favorable. In this section, we investigate the level of eigenstrain anisotropy required to overcome this effect and trigger short side bending.

When eigenstrains are equibiaxial, these parameters coincide with those used in Faucheux et al. (2018) which, closely resemble those used by Freund (2000) to characterize the response of thin film bilayers. In what follows, $\bar{B}$ and $\bar{\kappa}$ are referred to as the dimensionless load and the dimensionless curvature, respectively.

Figure 12 shows the evolution of dimensionless curvatures as a function of the dimensionless load for rectangular sheets of 1:1, 2:1, and 4:1 aspect ratio for $\chi = -6\,\%$, $0.1\,\%$, and $6\,\%$. These curves were obtained from finite element simulations using the same quarter plate model as described in Section 4. As in Section 4, the eigenstrains were applied uniformly. For $\chi = 0.1\,\%$, which corresponds to almost equibiaxial eigenstrains, simulations predict that all sheets bend preferentially along the long side, which is consistent with the analysis in Alben et al. (2011). For small dimensionless load (i.e., for small eigenstrain moments and/or thick plates), all sheets deform into spherical shapes. For larger dimensionless loads, out-of-plane deflections are no longer

25
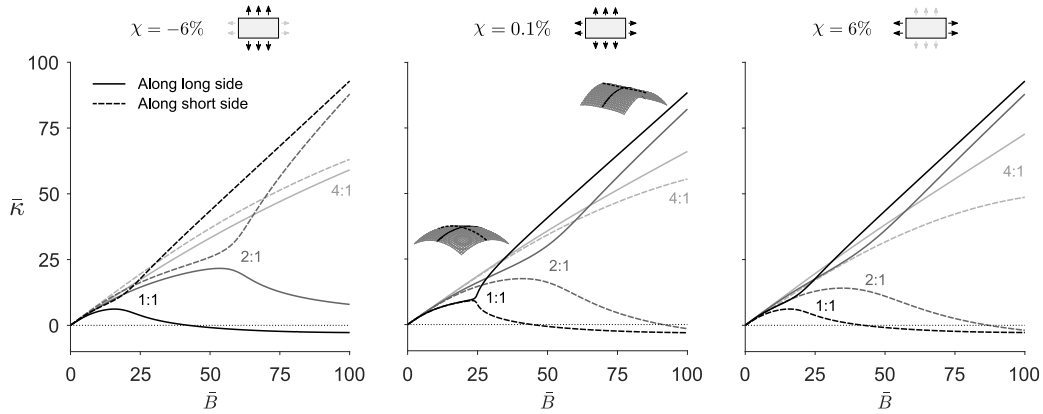
Figure 12. Master curves showing the relationship between dimensionless curvatures $\bar{\kappa}$ and dimensionless loads $\bar{B}$ for different levels of eigenstrain anisotropy χ for plates of 1:1, 2:1, and 4:1 aspect ratio. The curves were obtained by finite element simulations. For nearly equibiaxial eigenstrains (middle), square plates assume spherical shapes for dimensionless loads smaller than 25 then transition suddenly to an elliptical then cylindrical shapes due to an elastic instability. For all other aspect ratios and values of χ, the transition is gradual, and even more so as the strip is elongated or χ departs from 0. In the range of parameters considered here, plates always bend along the long side for $\chi > 0$ and they always bend along the short side for $\chi < -5\%$. For intermediate values of χ, the direction of largest curvature depends on the aspect ratio and on the dimensionless load.

small compared to the thickness and geometric nonlinearities become significant: the stress stiffening that results causes the curves to bend downward. Perfect 1:1 aspect ratio sheets maintain a spherical shape far into the nonlinear domain, up to a dimensionless load of about 25, then suddenly transition to cylindrical configurations due to an elastic instability. All other geometries display a smooth transition between spherical and cylindrical shapes with curvatures in the long and short directions gradually separating. Increasing χ only causes the curves to separate faster and the elastic instability for sheets of 1:1 aspect ratio to be replaced by a smooth transition. Decreasing χ, however, causes a sudden inversion of the bending direction for sheets of 1:1 and 2:1 aspect ratio. The transition occurs at $\chi = 0$ for the former, and at about $\chi = -5$ % for the latter. In other words, for sheets of 2:1 aspect ratio, the first eigenstrain moment along the short direction must be about 10 % larger than that along the long direction for eigenstrain anisotropy to overcome the geometric preference of the sheets to bend along the long side.

The value of the dimensionless parameters for our specimens can be deter-

26

Table 3

Dimensionless load $\bar{B}$ and eigenstrains anisotropy χ induced by all eigenstrains present in the specimens and by peening-induced eigenstrains only. The former were estimated from the curvature of the coupons while the latter where obtained by integrating previously identified eigenstrain profiles. Differences between the two sets of parameters are due to initial eigenstrains present below the peening-affected layer.

Specimen ID	Long side aligned with	All eigenstrains		Peening-induced eigenstrains only	
		$\bar{B}$ (-)	χ (%)	$\bar{B}$ (-)	χ (%)
Sheet 4:1–L	L	67	11.0	70.8	-4.4
Sheet 2:1–T	L	65	34.5	59.1	9.7
Sheet 1:1–L	-	66	23.7	61.5	7.6
Sheet 1:2–L	T	72	-18.6	67.0	-1.1
Sheet 1:4–L	T	66	-34.5	80.8	1.5

mined experimentally by noticing that, for a coupon small enough such that its response is not affected by geometric nonlinear effects,

$$B_i = \tilde{\kappa}_i h^3 / 12, \tag{23}$$

where $\tilde{\kappa}_i$ is the curvature of the coupon in the i direction (see Appendix A for details). The third and fourth columns of Table 3 list the values of $\bar{B}$ and χ thus computed from the curvatures of coupons used for residual stress measurements. In this case, $\bar{B}$ ranges from 65 to 72, χ is positive for specimens with their long side aligned with the L direction, and it is less than $-18\,\%$ for specimens with their short side aligned with the T direction. To put these values into perspective, the last two columns of Table 3 list the $\bar{B}$ and χ induced by peening-induced eigenstrains only—i.e., neglecting the contribution of initial eigenstrain present below the peening-affected layer. These values were obtained by integrating the previously identified near-surface eigenstrain profiles with Equation (18) from $z = 0$ to $z = d = 0.5$ mm. Whereas $\bar{B}$ does not markedly change, χ drops by several percent, even changing signs for sheets 4:1–L and 1:4–L. This shows that χ is quite sensitive to small variations in eigenstrains and that only slightly anisotropic eigenstrains are needed to overcome the geometric preference for the sheets to bend along the long side.

The competition between geometry and eigenstrain anisotropy is further illustrated by the map in Figure 13a which shows the direction of largest curvature as a function of the aspect ratio and χ at $\bar{B} = 70$. For perfect 1:1 aspect ratio plates, the boundary between the two regions is located at $\chi = 0$ and any small perturbation causes bending in either direction. The deformed shape on either side of the boundary are identical, but with the bending direction inverted, as illustrated in Figure 13b. For small aspect ratios, the boundary asymptotically approaches the $\chi = 0$ line. This is because the bending along the long side and the short side of a narrow plate become decoupled. In this domain, the curvature in one direction is simply proportional to the first eigenstrain moment in this direction and there is no sharp transition when crossing the boundary: curvature in both directions are almost identical when $\chi = 0$ and gradually separate when χ departs from zero. This is illustrated in Figure 13d which shows the deformed shape of 1:8 aspect ratio plates for $\chi = -2$ % (left) and $\chi = 2$ % (right). For intermediate aspect ratios, the boundary between the two regions moves towards negative χ since larger eigenstrains along the short direction are required to induce short side bending. The point the furthest away from the $\chi = 0$ line is reached for an aspect ratio of (approximately) 1:2.4, which suggests that the edge effects that favor long side bending described in Alben et al. (2011) are most pronounced for this specific geometry at $\bar{B} = 70$.

7. Conclusion

The purpose of this paper was to clarify how different sources of anisotropy contributed to the final deformed shape of 2024–T3 aluminum rectangular sheets shot peened to full coverage with steel shot 0.71 mm in diameter and propelled at 41 m s^{-1}. In particular, we tried to explain why sheets that were free to deform during peening always bent in the rolling direction of the alloy, no matter what their aspect ratio or their alignment with respect to the rolling direction was.

We analysed two sources of anisotropy likely to explain the observed deformed shapes: the plastic anisotropy of 2024–T3 aluminum, and the anisotropy of initial stresses inherited from the sheet manufacturing process. These residual stress initially present in the flat sheets redistribute when their equilibrium is disturbed by peening. The analysis of eigenstrain profiles identified from residual stress and curvature measurements showed no clear sign of ei-
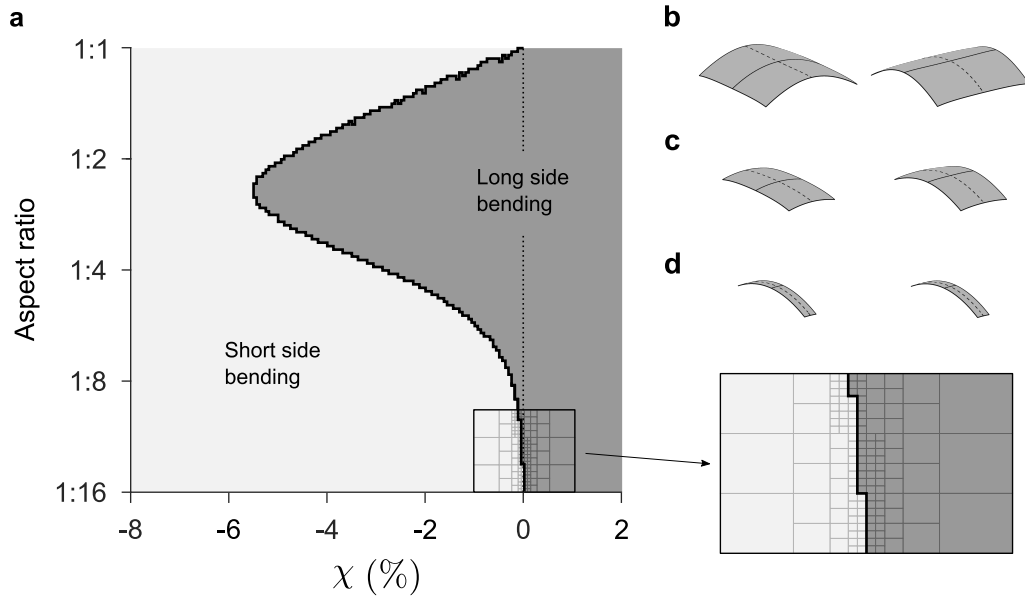
Figure 13. (a) Map showing the direction of largest curvature of rectangular plates of uniform thickness for $\bar{B} = 70$ and $\nu = 0.33$. The map is made of 3400 pixels, each pixel corresponding to one finite element simulation. The eigenstrains are larger along the long direction when $\chi > 0$ and vice versa. Plates of 1:1 aspect ratio and very elongated strips have their largest curvature in the direction along which the eigenstrains are the largest. For plates of intermediate ratio, there exist a domain in which the plates bend along their long side even when eigenstrains are largest along the short side. (b) Deformed shapes of plates of 1:1 aspect ratio for $\chi = \pm 1$ %, (c) of plates of 1:2 aspect ratio for $\chi = -6$ % and $\chi = -4$ %, and (d) of plates of 1:8 aspect ratio for $\chi = \pm 2$ %. Deflection magnified by a factor of 4.

ther mechanism prompting L side bending: peening-induced plastic strains were almost equibiaxial or slightly larger along the T direction—which would have favored T side bending—and bending moments induced by the rebalancing of initial stresses were one to two orders of magnitude smaller than those induced by the peening treatment. Further investigation revealed that the response of uniformly shot peened rectangular plates of uniform thickness is highly sensitive to small variations in internal loads and identified initial stresses as the most likely cause of L side bending. This sensitivity, however, is a feature of the simple geometries of the sheets and we believe that complex production parts such as pocketed or integrally stiffened panels should behave in a more controlled manner.

Once the sheets started to deform, significantly larger plastic strains developed in the bending direction. This effect is similar to that used in the variant of the process called stress peen forming where parts are held onto a curved jig during peening to obtain larger curvatures along the prestress direction. Whereas prestressed parts are firmly held into place during peening, the shape of unconstrained parts is continuously evolving; it depends on the precise peening sequence and on the geometry of the part. Capturing this effect in a numerical model of the process will likely require computer-intensive simulations. Alternatively, one could imagine implementing a feedback loop, possibly coupled to a learning system, to monitor the shape of a part as it is being peened and adjust the treatment accordingly. This kind of approach is well established in the industry (see for example Kittel et al. (1999); Lundquist et al. (2015)) but remains largely unexplored in the literature.

8. Acknowledgements

Appendix A. Estimating first eigenstrain moments from the curvature of small coupons

Consider a uniformly shot peened plate with a distribution of eigenstrains of the form in Equation (1). The first eigenstrain moments with respect to the *midplate* of the plate introduced in Equation (18), B_i, is related to the resulting eigenstrains, α_i, and the first eigenstrain moments with respect to the *surface* of the plate, β_i, through

$$B_i = \alpha_i h/2 - \beta_i. \tag{A.1}$$

Now, assume that a coupon is removed from the shot peened plate and that removal does not alter the distribution of eigenstrains. For example, imagine that a $254 \times 254 \times 4.9$ mm coupon is removed from a $1016 \times 1016 \times 4.9$ mm plate peen formed to a dimensionless load $\bar{B} = 70$. For $\bar{B} = 70$, the response of the plate is well into the nonlinear regime, as shown in Figure 12. However, since $\bar{B}$ scales with L^2, as in Equation (16), $\bar{B}$ drops to approximately 4.4 for the coupon, which is very nearly in the linear domain. In other words, removing a small coupon from a larger plate is a way to do away with geometric nonlinearities.

In the linear domain, the analytical solution presented in Section 3 applies. In particular, it can be used to express the α_i and β_i in terms of measurable quantities. For example, substituting Equations (15) and (9) in Equation (A.1) yields

$$B_i = \tilde{\kappa}_i h^3/12, \tag{A.2}$$

where a tilde is used to indicate that the curvatures are measured on the small coupon—and not directly on the plate.

References

References

P. A. Faucheux, H. Y. Miao, F. P. Gosselin, M. Lévesque, Peen forming and stress peen forming of 2024–T3 aluminum sheets: Part 1: 3D scans and residual stress measurements (2021). Manuscript submitted for publication to Strain.

K. M. Kulkarni, J. A. Schey, D. V. Badger, Investigation of shot peening as a forming process for aircraft wing skins, Journal of Applied Metalworking 1 (1981) 34–44.

S. Alben, B. Balakrisnan, E. Smela, Edge effects determine the direction of bilayer bending, Nano Letters 11 (2011) 2280–2285.

A. Korsunsky, A teaching essay on residual stresses and eigenstrains, 1st edition ed., Butterworth-Heinemann, Boston, MA, 2017.

T. Mura, Micromechanics of defects in solids, number 3 in Mechanics of Elastic and Inelastic Solids, 2 ed., Springer Netherlands, 1987.

T.-S. Jun, A. M. Korsunsky, Evaluation of residual stresses and strains using the Eigenstrain Reconstruction Method, International Journal of Solids and Structures 47 (2010) 1678–1686.

A. M. Korsunsky, On the modelling of residual stresses due to surface peening using eigenstrain distributions, The Journal of Strain Analysis for Engineering Design 40 (2005) 817–824.

Y. Hu, Z. Li, X. Yu, Z. Yao, Effect of elastic prestress on the laser peen forming of aluminum alloy 2024-T351: Experiments and eigenstrain-based modeling, Journal of Materials Processing Technology 221 (2015) 214–224.

F. Bron, J. Besson, A yield function for anisotropic materials Application to aluminum alloys, International Journal of Plasticity 20 (2004) 937–963.

J. Seidt, A. Gilat, Plastic deformation of 2024-T351 aluminum plate over a wide range of loading conditions, International Journal of Solids and Structures 50 (2013) 1781–1790.

M. B. Prime, Amplified effect of mild plastic anisotropy on residual stress and strain anisotropy, International Journal of Solids and Structures 118-119 (2017) 70–77.

B. Audoly, Y. Pomeau, Elasticity and geometry: from hair curls to the nonlinear response of shells, Oxford University Press, Oxford ; New York, 2010.

P. A. Faucheux, F. P. Gosselin, M. Lévesque, Simulating shot peen forming with eigenstrains, Journal of Materials Processing Technology 254 (2018) 135–144.

L. B. Freund, Substrate curvature due to thin film mismatch strain in the nonlinear deformation range, Journal of the Mechanics and Physics of Solids 48 (2000) 1159–1174.

S. Kittel, W. Linnemann, F. Wüstefeld, R. Kopp, Tight tolerance peen forming with on-line shape control, in: Proceedings of the 7th International Conference on Shot Peening (ICSP7), Warsaw, Poland, 1999, pp. 301–307.

L. K. Lundquist, M. A. Kunz, J. E. Pillers, J. B. Castle, J. Z. Lin, S. Nervi, Control feedback loop for real-time variable needle peen forming, 2015.